REPORT DOCUMENTATION PAGE

Form Approved
OMB No. 0704-0188

1. REPORT DATE *(DD-MM-YYYY)*	2. REPORT TYPE	3. DATES COVERED *(From - To)*
29-06-2015	Final	1 Mar 2014 - 31 Mar 2015; Jun 2015

4. TITLE AND SUBTITLE
Hydrodynamics Noise from Flexible Roughness Elements

5a. CONTRACT NUMBER

5b. GRANT NUMBER
N00014-14-1-0242

5c. PROGRAM ELEMENT NUMBER

6. AUTHOR(S)
Jaworski, Justin W
Daly, Conor
Peake, Nigel

5d. PROJECT NUMBER

5e. TASK NUMBER

5f. WORK UNIT NUMBER

7. PERFORMING ORGANIZATION NAME(S) AND ADDRESS(ES)
Lehigh University, 19 Memorial Drive West, Bethlehem, PA 18015

8. PERFORMING ORGANIZATION REPORT NUMBER

9. SPONSORING/MONITORING AGENCY NAME(S) AND ADDRESS(ES)
Office of Naval Research, 875 North Randolph Street, Arlington, VA 22203-1995

10. SPONSOR/MONITOR'S ACRONYM(S)
ONR

11. SPONSOR/MONITOR'S REPORT NUMBER(S)

12. DISTRIBUTION/AVAILABILITY STATEMENT
Approved for public release, distribution unlimited

13. SUPPLEMENTARY NOTES
Work supported in collaboration with NICOP grant N62909-12-1-7116 awarded to the University of Cambridge

14. ABSTRACT
The influence of a poroelastic surface structure composed of elastic fibers, as inspired by the wings of silent owl species, is investigated theoretically through the development of two mathematical models. First, in the spatial limit of a sparse distribution of fibers that are hydrodynamically uncoupled, the influences of fiber bending and a background flow on the far field sound are studied using conformal mapping. A second model reveals how the porous surface structure can suppress pressure fluctuations, which agrees well with companion experiments performed by Dr. William Devenport of Virginia Tech.

15. SUBJECT TERMS
vortex sound, flexible roughness, conformal mapping, porous canopy, Kelvin-Helmholtz instability

16. SECURITY CLASSIFICATION OF:			17. LIMITATION OF ABSTRACT	18. NUMBER OF PAGES	19a. NAME OF RESPONSIBLE PERSON
a. REPORT	b. ABSTRACT	c. THIS PAGE			Jaworski, Justin W
unclassified	unclassified	unclassified	SAR	15	19b. TELEPHONE NUMBER *(Include area code)* +1 (610) 758-4519

Award Information

Award Number	N00014-14-1-0242
Title of Research	Hydrodynamic Noise from Flexible Roughness Elements
Principal Investigator	Justin W. Jaworski
Organizations	Lehigh University

Technical Section

LONG-TERM GOALS & OBJECTIVES

Many owl species rely on specialized plumage to achieve functionally silent flight, which requires the suppression of aerodynamic noise for frequencies 2+kHz to not affect their acoustical targeting system and not alert prey of their approach. The specialized plumage features believed to be responsible for this noise suppression are a leading-edge comb of evenly spaced feathers, the velvety down material distributed over the upper wing surface, and a tattered and compliant trailing edge (see figure 1). Recent theoretical work by Jaworski and Peake [1] suggests that trailing-edge noise can be mitigated by the porous and elastic properties of the edge to the point where turbulence scattering by the edge scales similarly to roughness noise. If validated experimentally, this finding has broad implications for the design of quieter airframes and rotors, and the diminished edge noise implies that roughness noise has a more substantial contribution to the acoustic signature of specially-designed blades. Thus, the focus of the present research is to determine more precisely how these blades must be designed to achieve the desired turbulence noise reductions, and to model and assess how the novel surface roughness of owls may further contribute to tunable acoustic stealth.

In contrast to unique owl features at the leading- and trailing-edges, the velvety down is the least studied and most poorly understood component, which according to Lilley [2] is the feature that may offer the means to reduce the generation of turbulence noise at its source. The length scale of the owl down (~1mm) is inconsistent with the range of frequencies for a conventional acoustical absorber, thus the noise reduction mechanism is likely due to a novel coupled interaction between the flexible downy fibers with the fluid flow. In addition to determining theoretically and validating experimentally the parameter space where trailing-edge noise scales the same as or weaker than roughness noise, the present modeling effort at the University of Cambridge seeks to identify the salient parameters of roughness noise due to flexible surface elements. This effort seeks to establish an understanding of how the noise may be mitigated differently when the down is modeled either as a collection of individual flexible fibers or as a poroelastic continuum.

This project is part of a collaborative effort between Lehigh University, University of Cambridge (UK), Virginia Tech, and Florida Atlantic University. Incipient funding under the NICOP program (N62909-12-1-7116) to the University of Cambridge supported the theoretical analysis on the noise generation by flexible roughness by Drs. Nigel Peake and Justin Jaworski (now at Lehigh University). Researchers at Virginia Tech (Dr. William Devenport and graduate student Ian Clark) continue to carry out experimental work to test the developed trailing-edge and hydrodynamic flexible roughness theories and provide support for further theoretical developments. Dr. Stewart Glegg at the Florida Atlantic University advises the relationship between the theoretical and experimental results. The efforts at Virginia Tech and Florida Atlantic are the subject of a separate but coordinated project with ONR HQ. The overall objective of this combined effort is to evaluate and test the hypothesis that the soft owl down can suppress the unsteady surface pressure field on the scale of the roughness, either directly or indirectly through the modification of the turbulent structures of the boundary layer, and control not only the source of roughness noise but

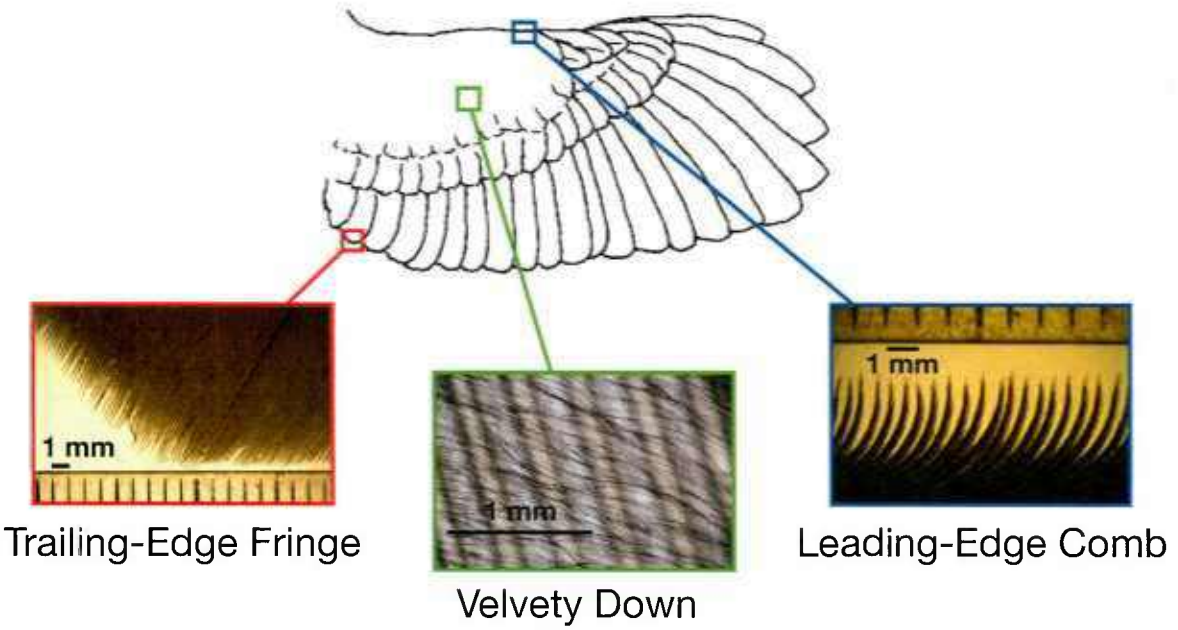

possibly also that of trailing edge noise and surface vibration.

At Lehigh University, this research effort has defined 2 months of summer work for Justin Jaworski, which has resulted in 2 conference papers and 1 patent application produced in collaboration with the international research team.

APPROACH

Analytical models for the suppression and generation of noise by the owl down material are developed and solved to gain insight into the essential physical mechanisms. For vortex noise generated by an inclined fiber, progress is made using conformal mapping techniques coupled with compact aeroacoustic Green's functions to find the far-field sound due to vortex motion. A separate analysis concerning noise suppression by the presence of a porous canopy involves the numerical solution of the two-dimensional Rayleigh equation using a standard Newton-Raphson numerical routine. Both theoretical analyses identify the dimensionless groups to furnish comparison with current and/or future experiments and computations.

WORK COMPLETED

Two theoretical models are developed to support the collaborative investigation of flexible roughness noise carried out with Cambridge, Virginia Tech, and Florida Atlantic universities. First, the problem of vortex sound produced by an inclined fiber in a mean flow was solved via conformal mapping techniques, whereby the computed vortex path generates a time-dependent signal in the acoustic far-field. This model furnishes a theoretical framework to understand the noise generation by owl down in its physical limit as a sparse collection of hydrodynamically-uncoupled fibers, enabling further work to take into account dynamic motions of the fiber and finite distances between fibers for more realistic aeroacoustic models of its turbulence noise generation.

Experimental measurements made at Virginia Tech indicate that a porous canopy can reduce surface pressure amplitudes by up to 30dB over a finite range of frequencies that depends linearly on the background flow speed. To examine the hypothesis that the porous layer creates an unstable wave near

the canopy by inflection of the boundary layer profile, a inflectional mixing-layer model is formulated and solved by numerical solution of the Rayleigh equation. Numerical solutions indicate that the boundary-layer inflection point is pushed upward towards the canopy, suggesting that a pure mixing-layer model without boundary-layer (no-slip) details may be sufficient to describe the most relevant physics. The semi-empirical model predictions for the porous canopy are in excellent agreement with low-frequency noise suppression trends. However, further work is necessary to include the proper physics into the model to improve the theoretical-experimental agreement at high frequencies.

RESULTS

1. Vortex Sound from Isolated Rigid Owl Down Fibers Inclined in a Mean Flow

The noise generation due to the interaction of the boundary-layer turbulence with the downy material is presently idealized as a vortex sound problem, where it is assumed that the downy material is sufficiently sparse such that its fibers are hydrodynamically uncoupled, and it is further assumed that these fibers are acoustically compact. The acoustical compactness of the fiber enables the use of the two-dimensional Green's function derived by Howe [3, p. 138] to relate the vortex path near the fiber to the resulting sound radiated to the acoustic far-field.

The mathematical analysis for sound due to a vortex passing round an inclined fiber follows the procedure outlined by Howe [3, pp. 193-194] for a vortex passing over a rigid, upright spoiler, which includes the effects of a background mean flow on the acoustic signal. We extend this work to allow for arbitrary angles of inclination with $\theta \in (0,1)$, as illustrated in Fig. 1, where the results of Howe are recovered for $\theta = 1/2$. The mapping from the z-plane to the ζ-plane is facilitated by using an elementary translation of the origin in the z-plane to the end of the spoiler, say, $z_1 = z + he^{-i\pi\theta}$, and then relating the z_1-plane to the ζ-plane by the Schwarz-Christoffel transformation [4,5].

$$z_1 = K\int_1^{\zeta} \frac{\chi - 1}{\chi^{1-\theta}(\chi - b)^{\theta}} d\chi \tag{1}$$

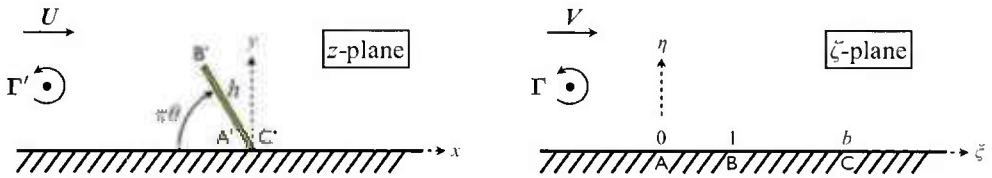

Figure 1. Vortex noise from an inclined fiber. *Conformal mapping relates the physical z-plane to the ζ-plane where the problem is solved. The impermeable wall condition is satisfied automatically by adding an appropriate image vortex to each plane.*

The constants K and b are determined by linking the maps between the z- and ζ-planes. For example, as $\zeta \to b$, $z_1 \to 0$, the same as for when $\zeta \to 0$. Applying these conditions to Eq. (1), and noting that a change of variable to $\tau = \chi / b$ transforms the integral into a beta function $\mathrm{B}(a,b)$ [6], these constants are found to be

$$b = 1/\theta, \tag{2}$$

$$K = \frac{h\sin\pi\theta}{\pi\left[I_\theta(\theta,1-\theta) - I_\theta(1+\theta,1-\theta)\right]} = \frac{h}{f(\theta)}, \tag{3}$$

where the incomplete beta function is defined by [6] ,

$$I_x(a,b)=\frac{\int_0^x \tau^{a-1}(1-\tau)^{b-1}\,d\tau}{\int_0^1 \tau^{a-1}(1-\tau)^{b-1}\,d\tau}=\frac{\mathrm{B}_x(a,b)}{\mathrm{B}(a,b)}. \tag{4}$$

Note that $f(\theta)=1$ in Eq. (3) in the special case of an upright fiber, $\theta=1/2$. The mapping relationship between the z- and ζ-planes is completed by equating the background mean flows far from the fiber, which yields $V=KU$.

The acoustic pressure due to vortex motion requires knowledge of the vortex path and the streamwise component of the Kirchhoff vector [3, pp. 52, 192]. The established nonlinear equations of motion for the vortex at $z_0(t)=x_0(t)+iy_0(t)$ are [3, p.107]

$$\frac{d\bar{z}_0}{dt}=\frac{dx_0}{dt}-i\frac{dy_0}{dt}=-\frac{i\Gamma}{4\pi}\frac{\zeta''(z_0)}{\zeta'(z_0)}+\left(\frac{i\Gamma}{2\pi}\frac{1}{\zeta(z_0)-\bar{\zeta}(z_0)}+UK\right)\zeta'(z_0), \tag{5}$$

where

$$\frac{\zeta''(z)}{\zeta'(z)}=\frac{1-\theta}{\theta}\left(\zeta(\zeta-1)(\zeta-1/\theta)\right)^{-1}\zeta'(z_0), \tag{6}$$

and

$$\zeta^{\theta}(\zeta-1/\theta)^{1-\theta}=\frac{z+he^{-i\pi\theta}}{K}-\left(\frac{1-\theta}{\theta}\right)^{1-\theta}e^{-i\pi\theta}, \tag{7}$$

can be found from Eq. (1) using the chain rule or via direct integration, respectively; the primes denote $(\,)'=d/dz$. In the special case of $\theta=1/2$, Eqs. (5-7) can be combined to yield equations of motion that are explicit in terms of the vortex position, z_0. However, in general, Eq. (5) depends implicitly on vortex position through $\zeta(z)$, which requires the solution of Eq. (7) for a given z. These vortex equations of motion (7) can be expressed in dimensionless form,

$$\frac{d\bar{Z}}{dT}=\left\{-if(\theta)\left[\frac{1-\theta}{\theta}\frac{1}{\zeta(z_0)\left(\zeta(z_0)-1\right)\left(\zeta(z_0)-1/\theta\right)}-\frac{2}{\zeta(z_0)-\bar{\zeta}(z_0)}\right]+\varepsilon\right\}\zeta^{1-\theta}(z_0)\left(\zeta(z_0)-1\right)^{-1}\left(\zeta(z_0)-1/\theta\right)^{\theta}, \tag{8}$$

using the following dimensionless groups:

$$Z=\frac{z_0}{h},\ S=\frac{\Gamma}{4\pi h},\ T=\frac{tS}{h},\ \varepsilon=\frac{U}{S}. \tag{9}$$

The component of the Kirchhoff vector in the streamwise direction is simply the real part of the complex velocity potential for unit speed ($U=1$) in the z-plane, i.e. $\mathrm{Re}(K\zeta)$. Howe [3, p. 193] defines a function,

$$W(Z)=\frac{d}{dz}(K\zeta)=\zeta^{1-\theta}(\zeta-1)^{-1}(\zeta-1/\theta)^{\theta}, \tag{10}$$

such that the acoustic pressure in the far-field due to the vortex motion is

$$\frac{p(\mathbf{x},t)}{\rho_0 S^2 \sqrt{M}\sin\phi\left(h/\|\mathbf{x}\|\right)^{1/2}} \approx 2^{5/2}\frac{\partial}{\partial T}\int_0^{\infty}\mathrm{Im}\left[W(Z)\frac{dZ}{d\hat{T}}([T]-\lambda^2)\right]d\lambda\,, \tag{11}$$

where the second term in the integrand implies the function dependence $\frac{dZ}{d\hat{T}}([T]-\lambda^2)=u([T]-\lambda^2)+iv([T]-\lambda^2)$ and $\hat{T}=[T]-\lambda^2$. Equation (11) measures the acoustic pressure at far-field location $\mathbf{x}$, which is inclined at an angle ϕ measured clockwise from the y-direction. In Eq. (11), ρ_0 is the stationary fluid density, c_0 is the isentropic speed of sound, the Mach number is defined as $M=V/c_0$, and $[T]$ is the nondimensional retarded time.

The vortex path and acoustic pressure are evaluated numerically using Eqs. (5) and (11), respectively. The initial location of the vortex is sufficiently far upstream that its initial motion is undisturbed by the fiber; in this study, the initial vortex position is set to $Z=-10+0.75i$. Figure 2 illustrates these vortex paths for θ=1/3, 1/2, and 2/3 and in the cases with (ε=1) and without (ε=0) a background mean flow. Curiously, the vortex path is pushed upwards by the fiber at greater distances than the respective no-flow cases regardless of the fiber angle. Nonetheless, the effect of a mean flow is to draw the vortex path nearer to the edge of the fiber as it passes over, resulting in a louder sound seen in comparison of Figs. 3 and 4. Figures 3 and 4 show the reduced acoustic pressure from Eq. (11) as a function of the non-dimensional retarded time, where $[T]$=0 refers to the instant where the point vortex crosses the line extending from the end of the fiber. The cases for θ=1/2 replicate the existing results in the literature [3, 7] and verify the new approach presented here that is able to handle arbitrary angles of the fiber.

A comparison of the cases θ=1/3 and 2/3 in Fig. 4 indicates that leaning the fiber against the flow produces a greater positive pressure as the vortex nears the end of the fiber, and leaning the fiber with the flow reduces the positive pressure peak but increases the magnitude of the negative peak, as one would expect intuitively. However, Fig. 3 shows surprisingly that the same trend exists without a background flow, indicating that the presence of a mean flow is not responsible for the relative shifts of the pressure peaks, although a mean flow certain increases the magnitudes of these peaks.

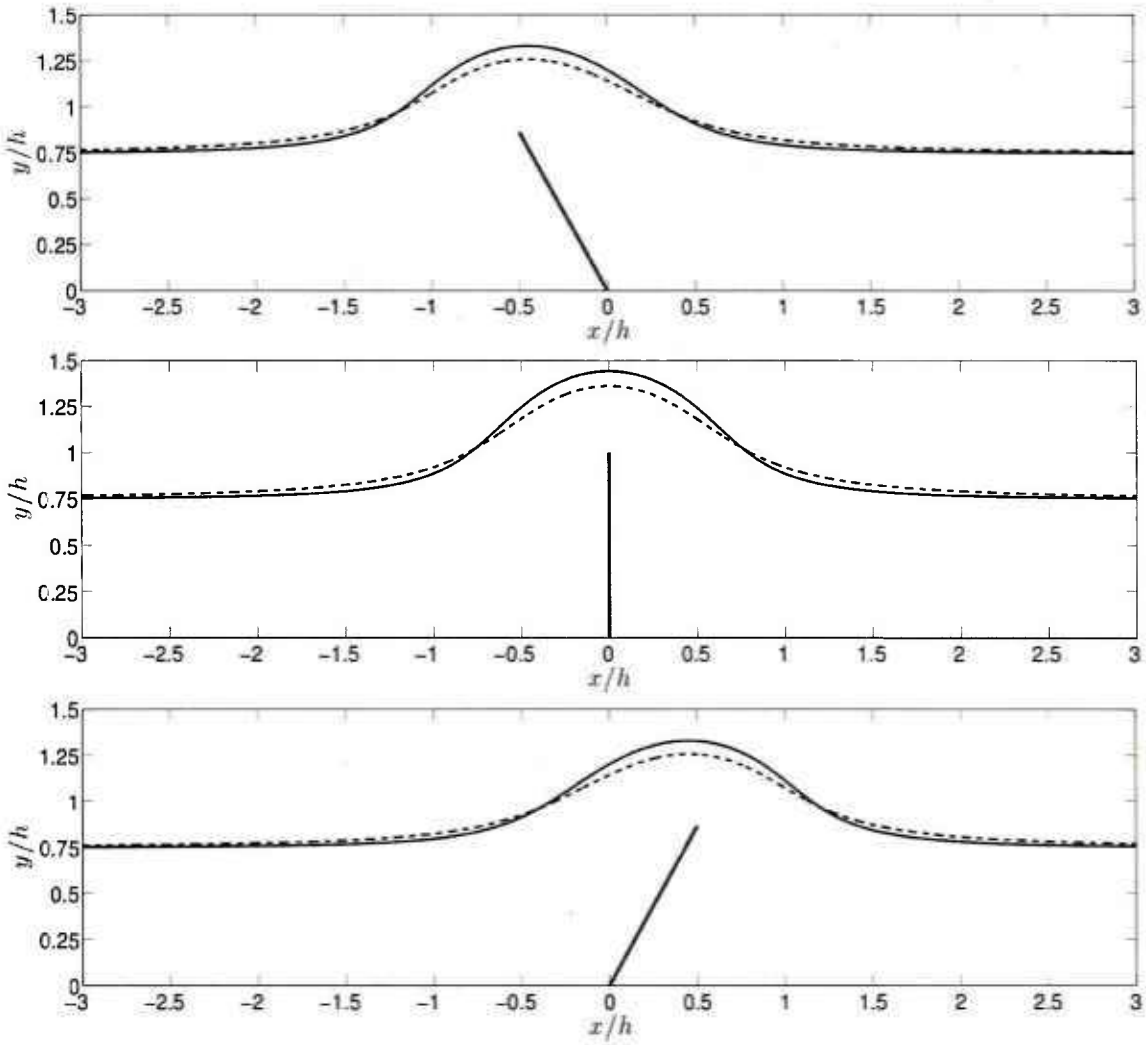

Figure 2. Vortex paths round a rigid inclined fiber. *The self-induced vortex paths show the influence of the fiber inclination and background mean flow on the vortex trajectory. θ =1/3 (top), 1/2 (middle), 2/3 (bottom). The trajectories for $\varepsilon = 0$ and $\varepsilon = 1$ are indicated by the solid and dashed lines, respectively.*

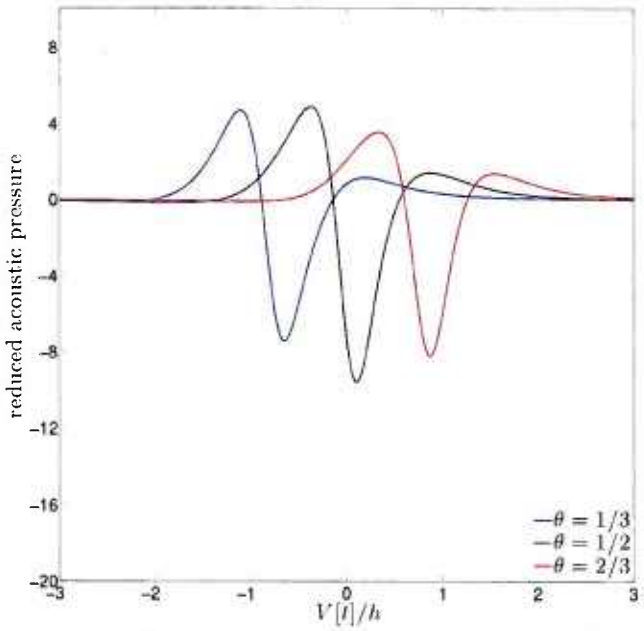

Figure 3. Vortex noise signature without background flow ($\varepsilon = 0$). *Results for θ = 1/3, 2/3 show that the inclination of the rigid fiber towards the incoming vortex increases the acoustic pressure values at the peaks. The present methodology is validated by the results of Howe [14] for θ = 1/2. The retarded time is taken with respect to the instant when the vortex passes through the line extending from the fiber.*

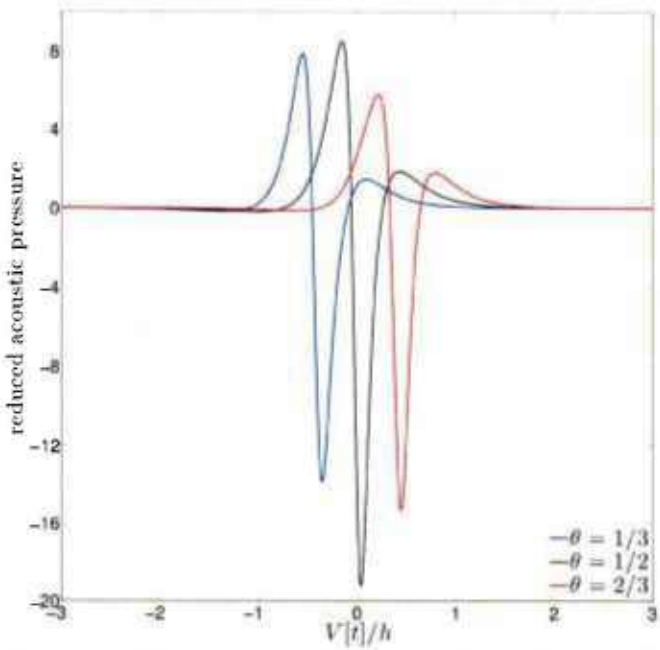

Figure 4. Vortex noise signature with background flow ($\varepsilon = 1$). *The background flow greatly enhances both the magnitude and approximately doubles the frequency of the vortex noise signature. The previous work by Howe [14] is confirmed for θ = 1/2. The retarded time is taken with respect to the instant when the vortex passes through the line extending from the fiber.*

2. Canopy Mixing-Layer Instability and Noise Suppression

A tentative model is proposed to explain features of the reduction in unsteady surface pressure levels which result from introduction of the fabric covering. First, Fig. 5 plots the decibel reduction in the experimental surface pressure spectrum between the datum uncovered case and the case with the covering in place, for several different wall-jet flow speeds. Interestingly, the shapes of the curves are remarkably similar to each other. In each case there is a definite maximum reduction, whose amplitude is inversely proportional to U_{jet} and which occurs at a frequency which is proportional to U_{jet}, i.e. at constant Strouhal number. Moreover, he canopy is only effective in reducing the surface pressure spectrum over a finite range of frequencies $f_{\text{cut-on}} < f < f_{\text{cut-off}}$ say, with both cut-on and cut-off frequencies, $f_{\text{cut-on}}$ and $f_{\text{cut-off}}$, increasingly linearly with U_{jet}.

Our inspiration for modeling this effect comes from studies of air flow over forest canopies (see [8,9] for a review), where it is well known that the drag of the canopy retards the lower portion of the atmospheric boundary layer, leading to an inflectional profile which undergoes a classical mixing-layer instability [10] – the so-called canopy instability. We hypothesize that the introduction of the fabric canopy has the same effect on the wall-jet boundary layer.

The next step in our argument is to note that shear instability leads to exponential growth in the streamwise direction, but exponential decay in the direction transverse to the shear layer. This effect can be seen most simply in the case of Helmholtz instability of a vortex sheet: for a shear of strength U at frequency ω, the Kelvin-Helmholtz wave has exponential spatial growth rate ω/U and decays with transverse distance at exponential decay rate ω/U. The vortex sheet is of course unstable at all frequencies and its spatial growth rate is unbounded. However, a genuine, finite-thickness, shear layer will typically only be spatially unstable over a finite frequency range, and will typically have a definite frequency at which a maximum growth rate (and therefore by analogy with Kelvin-Helmholtz a maximum transverse decay rate) occurs. Moreover, the characteristic frequencies of the shear layer will often occur at approximately constant Strouhal number. These features are very much in tune with the features of the experimental results described in the first paragraph. Our hypothesis for the effect of the canopy is therefore as follows: the canopy introduces an inflectional profile, which leads to instability waves (as nascent turbulent eddies), which, due to the presence of the canopy, are lifted higher above the solid boundary than they would have been without the canopy present. The pressure footprint of these eddies on the solid surface is therefore (substantially reduced), by both the transverse exponential decay effect of the instability wave and by their greater stand-off from the wall.

In order to investigate our hypothesis further, we now consider the stability of a simple inflectional boundary layer above a wall, and compute the spatial growth rates of the system for varying frequency. Specifically, we investigate the spatial instability of the piecewise linear boundary layer, with a base flow which approximates a general parallel boundary layer using straight line-segments. Velocities and lengths are non-dimensionalized in terms of the free-stream velocity U_s and the boundary layer thickness h. In terms of the wall-normal coordinate y, the boundary layer velocity profile is written as

$$U(y) = \begin{cases} \dfrac{by}{\delta} & 0 \le y < \delta, \\ \dfrac{(1-b)y + b - \delta}{1-\delta} & \delta \le y < 1, \\ 1 & y \ge 1. \end{cases}$$

Here $0 < \delta < 1$ controls the wall-normal location at which the line segments change their slope, and $0 < b < 1$ determines the gradient of the velocity profile in the two regions beneath $y = 1$. An example

profile is given in Fig. 6. The condition for the profile to be inflectional, and therefore inviscidly unstable, is $b < \delta$. This system is a generalization of the case treated in [11], which corresponds to $\delta = 1/2$ in our notation.

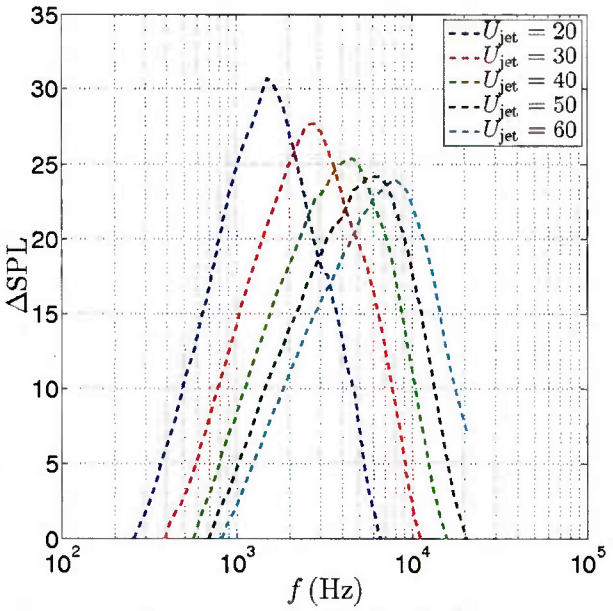

Figure 5. Experimental surface pressure level reductions due to canopy introduction.

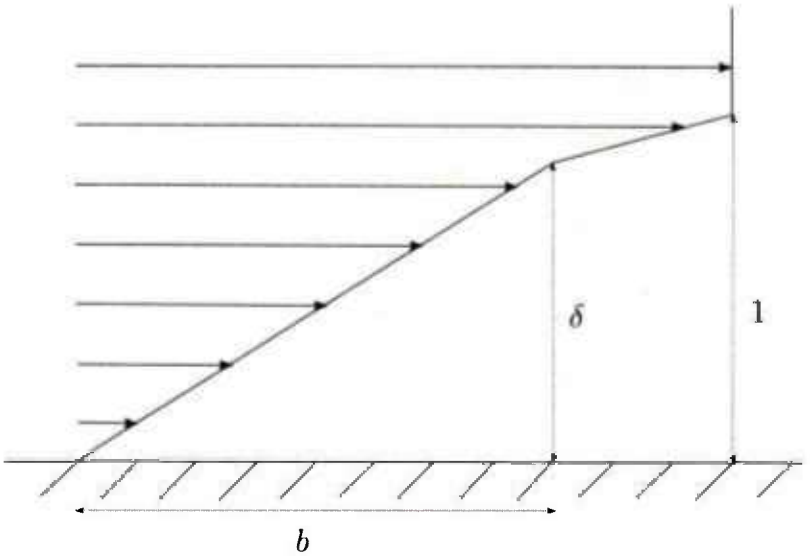

Figure 6. Schematic of the piecewise linear boundary layer.

To determine the spatial stability of the base flow $U(y)$ we first assume wavelike, two-dimensional velocity and pressure perturbations of the form

$$[\tilde{u}, \tilde{v}, \tilde{p}](x, y, t) = [u, v, p](y)e^{ikx - i\omega t},$$

where x is the streamwise coordinate, $\omega \in \mathbb{R}$ is the temporal frequency and $k \in \mathbb{C}$ is the streamwise wavenumber. Thus spatially unstable modes have $\mathrm{Im}\{k\} < 0$. Perturbations of this form satisfy the Rayleigh equation

$$(\omega - kU)(D^2 - k^2)v - U''v = 0,$$

where $D = d/dy$. Since $U(y)$ is linear in y, and since $k \in \mathbb{C}$, the Rayleigh equation simplifies to

$$(D^2 - k^2)v = 0.$$

This simplification allows us to determine an exact dispersion relation $d(\omega, k, b, \delta)$. Assuming a wall-normal velocity perturbation profile which satisfies the Rayleigh equation in each of the three mean profile regions gives

$$v(y) = \begin{cases} Ae^{-ky} + Be^{ky} & 0 \le y < \delta, \\ Ce^{-ky} + De^{ky} & \delta \le y < 1, \\ Ee^{-ky} & y > 1, \end{cases}$$

for $\mathrm{Re}\{k\} > 0$. We can solve for $d(\omega, k, b, \delta)$ by elimination of the constants A, B, C, D, E. These constants are eliminated by imposing zero wall-normal flow at the lower wall, and jump conditions at δ and 1 which impose continuity of pressure and wall-normal velocity. Using $[\![.]\!]$ to denote jump conditions, we have

$$\begin{gathered} v(0) = 0, \\ [\![(\omega - kU)Dv + kU'v]\!] = 0, \\ \left[\!\!\left[\frac{v}{\omega - kU}\right]\!\!\right] = 0. \end{gathered}$$

In this manner, we derive the four parameter, nonlinear dispersion relation

$$d(\omega, k, b, \delta) = \alpha\omega^2 + \beta\omega + \gamma,$$

where, using $\xi = \coth(k\delta)$, we have defined

$$\begin{aligned} \alpha &= 2(1 + \xi), \\ \beta &= (1 + \xi)\left(\frac{1 - b}{1 - \delta} - 2k(1 + b)\right) + \frac{2(b - \delta)}{\delta(1 - \delta)} - \left(\frac{(1 - \xi)(1 - b)}{1 - \delta}\right)e^{-2k(1-\delta)}, \\ \gamma &= \left(bk(1 + \xi) + \frac{\delta - b}{\delta(1 - \delta)}\right)\left(2k - \frac{1 - b}{1 - \delta}\right) + \left(\frac{1 - b}{1 - \delta}\right)\left(\frac{\delta - b}{\delta(1 - \delta)} - bk(1 - \xi)\right)e^{-2k(1-\delta)}. \end{aligned}$$

Solutions k of $d(\omega, k, b, \delta) = 0$ are found via Newton iteration, where the derivative $\partial d/\partial k$ is computed at each step from an analytic expression.

The theoretical framework presented above is now used to attempt to reproduce, as far as possible, the experimental results. In order to do this, we will make sensible choices for some of the parameters in our model which can be estimated (such as the jet speed and the canopy height). However, other parameters (such as the effective strength and position of the inflection point) are harder to estimate, and instead we will try to tune the free parameters b and δ in order to try and fit the results. We are therefore not attempting, at this stage, to make a complete quantitative prediction without the need for any fitting, but

rather we wish to determine whether or not the canopy instability model is capable of recovering the features seen in experiment.

To facilitate experimental comparison, the boundary layer thickness in our model is taken to be the canopy height $h = h_c = 4\text{mm}$. The velocity above the canopy is observed experimentally to be about one third of the total jet velocity, so accordingly our free-stream velocity is chosen as $U_s = U_{\text{jet}}/3$. Frequencies f in Hertz can then be mapped to non-dimensional frequencies using the relation

$$\omega = \frac{6\pi f h_c}{U_{\text{jet}}}.$$

For each U_{jet}, the parameters b and δ are tuned by matching the cut-on, $\omega_{\text{cut-on}}$, and maximum, ω_{max}, frequencies of the instability growth rate

$$\text{Im}\{k(\omega_{\text{cut-on}})\} = 0, \quad \text{Im}\{k(\omega < \omega_{\text{cut-on}})\} > 0,$$
$$\min_{\omega} \text{Im}\{k(\omega)\} = \text{Im}\{k(\omega_{\text{max}})\},$$

with the experimental values $\omega_{\text{cut-on}}^{\text{exp}}$ and $\omega_{\text{max}}^{\text{exp}}$. We optimize over b and δ to satisfy the relative error constraint

$$r_{\text{err}} = \left(1 - \frac{\omega_{\text{cut-on}}}{\omega_{\text{cut-on}}^{\text{exp}}}\right)^2 + \left(1 - \frac{\omega_{\text{max}}}{\omega_{\text{max}}^{\text{exp}}}\right)^2 < 10^{-6}.$$

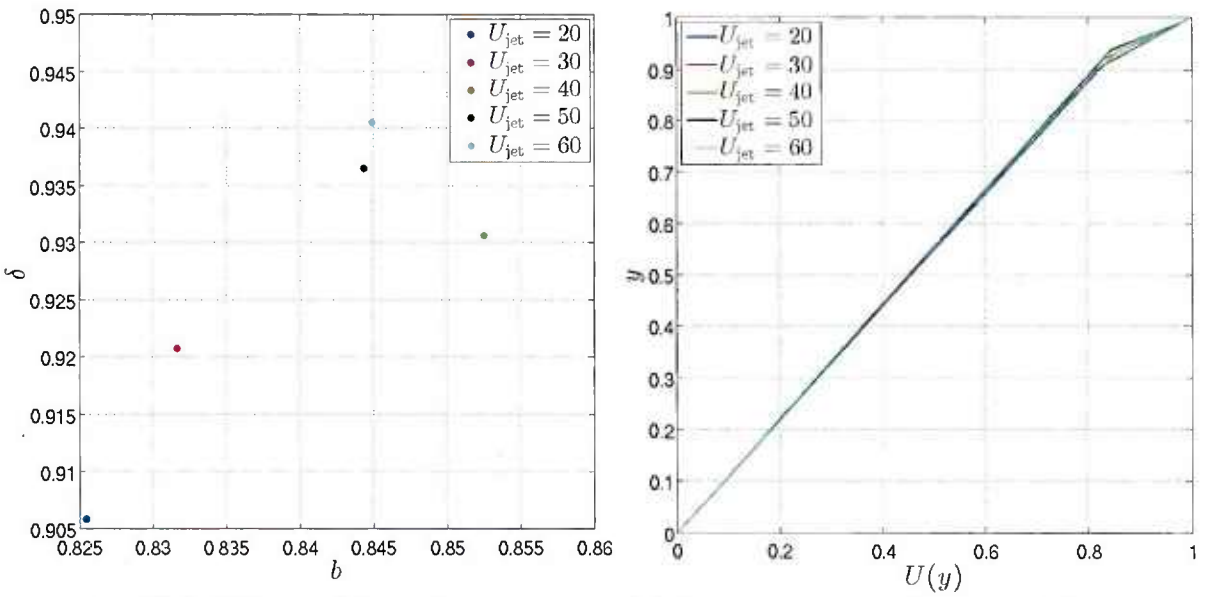

Figure 7. (a) optimized b and δ for each jet speed. (b) boundary layer profiles for each case.

Results of the optimization are shown in Fig. 7, where it can be seen that the optimal b lie in the range $0.825 < b < 0.855$ and the optimal δ are scattered between $0.905 < \delta < 0.945$. We plot the growth rates $-\text{Im}\{k\}$ in Fig. 8.

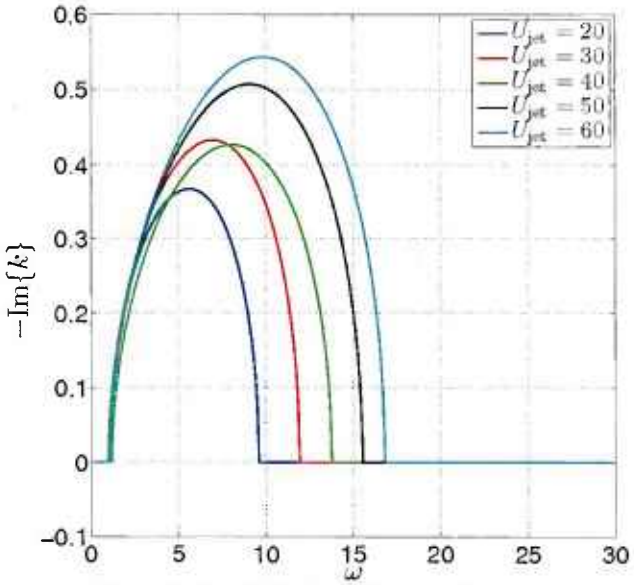

Figure 8. Spatial instability growth rates.

The pressure eigenfunctions for each unstable eigenvelocity can be computed using the relation

$$p = \frac{i}{k^2}\left((\omega - kU)Dv + \left(\frac{bk}{\delta}\right)v\right).$$

Examples for cases close to the cut-on and maximum frequencies are plotted in Fig. 9. Note in Fig. 9(a) that the pressure-amplitude of the instability wave changes little between just above the canopy and the wall, in the cut-on case. However, there is significant attenuation in the least stable case, seen in Fig. 9(b), in support of our assertion that the presence of the canopy shields the wall from the presence the pressure fluctuations in the upper boundary layer.

In order to compare more directly with the SPL attenuation data, we suppose that the change in SPL is related to the linear instability in the following manner

$$\Delta\text{SPL} = 20\log_{10}\left(e^{-\text{Im}\{k\}d_h}\right),$$

where we define d_h to be the pressure instability length scale, i.e. the height above the wall where the least stable linear wave is located in order to fix the level of attenuation observed in the experiment. For each jet speed, we determine d_h using the maximum instability growth rate and the maximum SPL fluctuation

$$d_h = \frac{1}{(-\text{Im}\{k\})_{\max}}\log\left(10^{\frac{\Delta\text{SPL}_{\max}}{20}}\right).$$

In Fig. 6(a) we plot the value d_h takes at each jet speed, and in Fig. 6(b) we contrast our ΔSPL estimate with the experimental quantities.

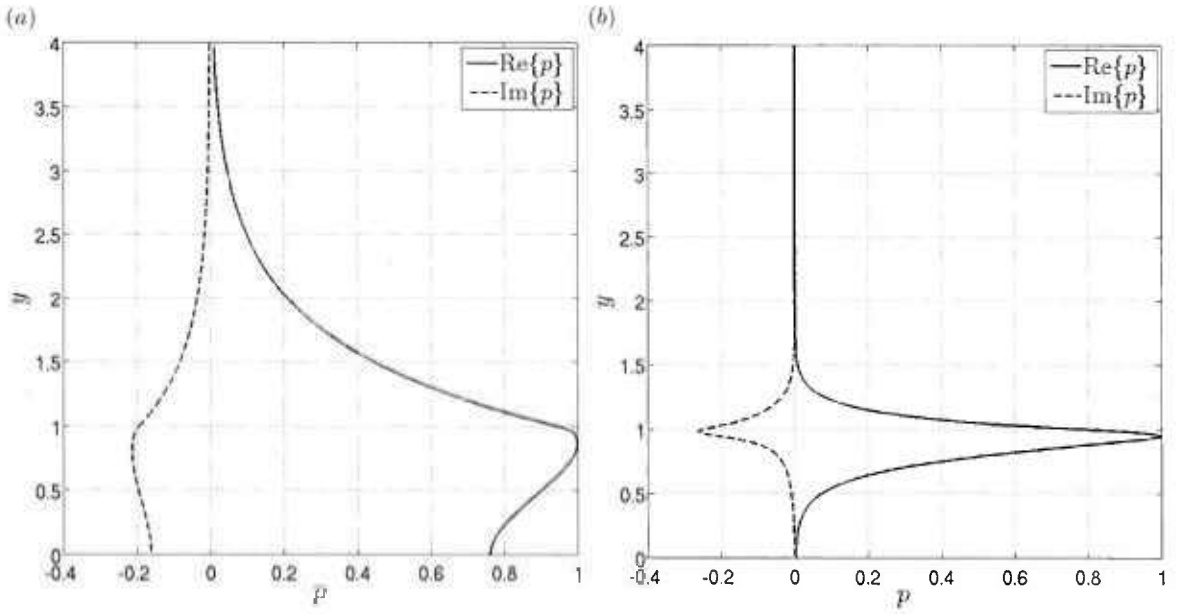

Figure 9. Pressure eigenfunctions for $U_{\text{jet}} = 40$ (a) $\omega = 1.2$ (b) $\omega = 8.05$.

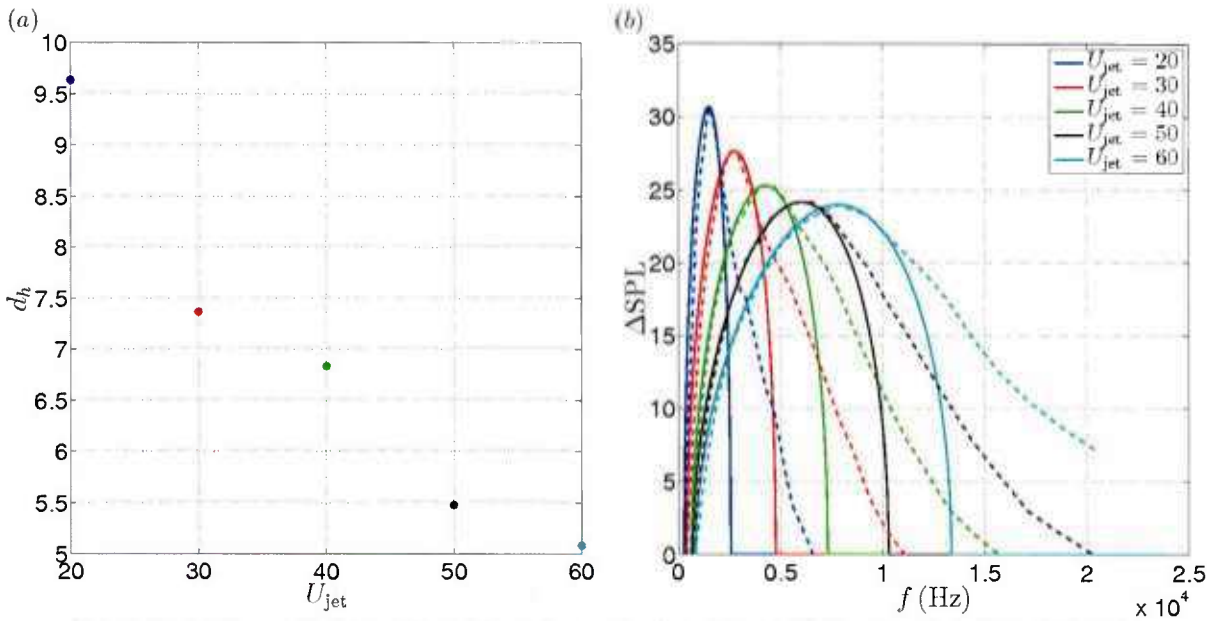

Figure 10. (a) values of the pressure instability length and (b) our ΔSPL estimate (solid) against the experimentally observed values (dashed).

What becomes apparent in Fig. 10(b) is that the canopy-instability model is capable, for suitably chosen parameter values, of capturing aspects of the canopy attenuation, specifically the lower-frequency cut-on behavior and the maximum attenuation. However, although the canopy-instability model does indeed predict a maximum frequency (and captures the right trend with varying speed), the predicted value of the maximum frequency differs significantly from the experimental value. Indeed, it is clear that the experimental attenuation curves differ in shape from the canopy-instability curves above a certain speed-

dependent frequency (note the 'shoulder' in each experimental curve), which suggests that some other mechanism takes over at higher frequency. Elucidation of this other mechanism is a matter for further research.

IMPACT/APPLICATIONS

The theoretical models developed through this project offer insight into the noise suppression behavior of individual fibers and porous canopies, which may impact further research into turbulence noise generation and its interactions with more sophisticated poroelastic wall structures.

The international research collaboration led to the development of streamwise-oriented surface structures termed "finlets," which have not been included in this report due to its patent application status. Our finlet designs have been demonstrated experimentally to yield trailing-edge noise suppression levels of up to 10dB over a broad range of angles of attack with minimal impact on the aerodynamic lift and drag characteristics. The physics mechanisms underpinning the finlet design are not completely understood and remain the subject of continued theoretical and experimental investigations.

REFERENCES

[1] Jaworski JW, Peake N. 2013 Aerodynamic noise from a poroelastic edge with implications for the silent flight of owls. *J. Fluid Mech.* 723:456-479.

[2] Lilley GM. 1998 A study of the silent flight of the owl. *AIAA Paper* 1998-2340.

[3] Howe MS. 2003 *Theory of Vortex Sound.* Cambridge Univ Press.

[4] Milne-Thompson LM. 1968 *Theoretical Hydrodynamics*, 5th ed, Dover, New York, Chap. 10.

[5] von Koppenfels W, Stallmann F. 1983 *Praxis der konformen Abbildung*, 2nd ed, Springer-Verlag, Berlin, pp. 212-213.

[6] Abramowitz M, Stegun IA. 1972 *Handbook of Mathematical Functions with Formulas, Graphs, and Mathematical Tables*, 10th printing, National Bureau of Standards, pp. 258, 263.

[7] Abou-Hussein H, Debenedictus A, Harrison N, Rodrigues MA, Zagadou F, Howe MS. 2002 Vortex-surface interaction noise: a compendium of worked examples. *J. Sound Vib.* 252(5):883-918.

[8] de Langre E. 2008 Effects of Wind on Plants, *Annu. Rev. Fluid Mech.* 40:141-168.

[9] Finnigan J. 2000 Turbulence in plant canopies. *Annu. Rev. Fluid Mech.* 32:519–71

[10] Raupach MR, Finnigan JJ, Brunet Y. 1996 Coherent eddies and turbulence in vegetation canopies: the mixing-layer analogy. *Bound. Layer Meteorol.* 78:351–82

[11] Schmid PJ, Henningson DS. 2001 *Stability and Transition in Shear Flows*, Springer, Chap. 2.

PUBLICATIONS

Clark IA, Devenport W, Jaworski JW, Daly C, Peake N, Glegg S. The noise generating and suppressing characteristics of bio-inspired rough surfaces. Proceedings of 20th AIAA/CEAS Aeroacoustics Conference, Atlanta, GA, 16–20 June 2014. Paper AIAA-2014-2911.

Clark IA, Alexander WN, Devenport WJ, Glegg SA, Jaworski JW, Daly C, Peake N. Bio-inspired trailing edge noise control. Proceedings of 21st AIAA/CEAS Aeroacoustics Conference, Dallas, TX, 22–26 June 2015. Paper AIAA-2015-2365.

PATENT

Alexander WN, Clark IA, Devenport WJ, Glegg SAL, Jaworski JW, Peake N, Daly C. Noise reducing surface treatment for airfoil. International Patent Application PCT/US14/59508.

HONORS/AWARDS/PRIZES

2015 AFOSR Young Investigator Award (Justin Jaworski, Lehigh University)